Chinese Chemical Letters 37 (2026) 110975

Contents lists available at ScienceDirect

Chinese Chemical Letters

journal homepage: www.elsevier.com/locate/cclet

Pseudo-mono-coordinate dysprosium(III)-alkoxide complexes exhibit enhanced magnetic axiality and blocking temperature

Wen-Jie Xu[a,1], Qian-Cheng Luo[a,1], Yang Fang[a], Chen-Jie Yuan[b], Jin-Tao Lu[c,d], Yuan-Qi Zhai[a,b,*], Yu Wang[b,*], Yan-Zhen Zheng[a,b,*]

[a] *Frontier Institute of Science and Technology (FIST), State Key Laboratory of Electrical Insulation and Power Equipment, Xi'an Key Laboratory of Electronic Devices and Material Chemistry, School of Chemistry, Xi'an Jiaotong University, Xi'an 710054, China*
[b] *MOE Key Laboratory for Non-Equilibrium Synthesis and Modulation of Condensed Matter, School of Physics, Xi'an Jiaotong University, Xi'an 710049, China*
[c] *Key Laboratory of the Ministry of Education and International Center for Dielectric Research, School of Electronic Science and Engineering, Xi'an Jiaotong University, Xi'an 710049, China*
[d] *Xi'an SIMOLDE Science and Technology Co., Ltd., Xi'an 710049, China*

ARTICLE INFO

Article history:
Received 7 December 2024
Revised 7 February 2025
Accepted 18 February 2025
Available online 18 February 2025

Keywords:
Single-molecule magnets
Pseudo-mono-coordinate
Alkoxide
Dysprosium
Axiality

ABSTRACT

Synthesis of *pseudo*-mono-coordinate dysprosium(III) single-molecule magnets (SMMs) with strong axiality is challenging. Here, by using very basic alkoxides as axial ligands and ether type neutral ligands as ancillary parts two targeted complexes, $[Dy(O^tBu)(15\text{-}C\text{-}5)(THF)_2][I_3]_2$ **1** and $[Dy(1\text{-}AdO)(15\text{-}C\text{-}5)(THF)_2][I_3]_2$ **2** were successfully isolated. Structurally they possess very short $Dy–O_{alkoxide}$ bonds (2.016(4) Å for **1** and 2.028(3) Å for **2**) and very long $Dy–O_{ether}$ bonds (ranging from 2.427(4) Å to 2.523(4) Å for **1** and 2.416(3) Å to 2.509(3) Å for **2**). As such, they are very similar to the diatomic model complex $[DyO]^+$and can be magnetically perceived as pseudo-mono-coordinate Dy(III) complexes. Both **1** and **2** exhibit high effective magnetic anisotropy barriers (1054(6) K for **1** and 1028(9) K for **2**). Consequently, both **1** and **2** demonstrate high opening hysteresis temperatures, namely 14 K for **1** and 10 K for **2**. This study provides a new insight into of pseudo-mono-coordinate mode and further emphasizes the excellent potential of this model for constructing high-performance SMMs.

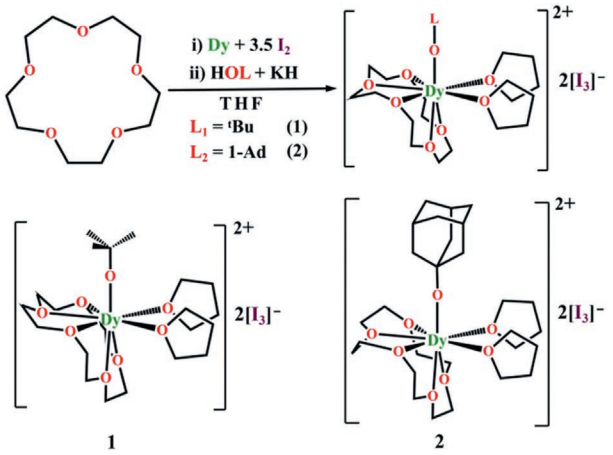
© 2026 Published by Elsevier B.V. on behalf of Chinese Chemical Society and Institute of Materia Medica, Chinese Academy of Medical Sciences.

Single-molecule magnets (SMMs) have attracted much attention to scientists working in the fields of chemistry, physics and materials science since the first appearance [1], owing to the potential applications in high density data storage [2,3], molecular spintronics [4,5] and quantum information processing [6–8]. In this context, the enhancement of effective energy barrier (U_{eff}) to magnetization reversal and blocking temperature (T_B) is the prerequisite. Notable progress has been achieved with lanthanide complexes, particularly for Dy(III) based complexes, owing to the large magnetic anisotropy derived from the $^6H_{15/2}$ ground-state term with large orbital momentum [9–11]. However, such a ground term has to be splitted by axial crystal field in order to maximize the magnetic anisotropy. Thus, two types of ligands are shown to exert such effect. The first one is cyclopentadienyl (Cp) based ligands which uses the η^5-pentadentate coordination mode to sandwich the central Dy(III) ions. The $Cp_{cent}–Dy–Cp_{cent}$ bending usually determines the axiality of the complexes [12–21]. Hence, bulky substituted Cp ligands demonstrate higher U_{eff} and T_B of these complexes [21]. In contrast, the second family which has more straight coordination mode of L–Dy–L and pseudo-D_{nh} local symmetry depending on the coordination number of the equatorial ligands [22–36]. Such a family could be termed as "the pseudo-two-coordinate family", in which the $[Dy(18\text{-}C\text{-}6)(1\text{-}AdO)_2][I_3]$ complex exhibits a benchmark U_{eff} of 2437(19) K [36].

In addition to the *pseudo*-two-coordination model, mono-coordinate Dy(III) complexes are also effective to enhance U_{eff}. The extreme case is the gas type $[DyO]^+$ model cation with a Dy-O bond length of only 1.74 Å, and its U_{eff} was predicted to be larger than 3000 K [37]. However, in reality $[DyO]^+$ is not isolable and only those with "*pseudo*-mono-coordinate" Dy(III) complexes are designable. In this context, several *pseudo*-mono-coordinate Dy(III) complexes with axial Dy–F/N/O bonds have been reported (Table S1 in Supporting information) [38–42]. The complex $[Dy(Tp^{py})F(dioxane)](PF_6)$ bearing single of Dy–F bond exhibits U_{eff} exceeding 600 K [38]. Constructing Dy–N complexes requires

* Corresponding authors.
E-mail addresses: zhaiyuanqi@xjtu.edu.cn (Y.-Q. Zhai), yuwang@mail.xjtu.edu.cn (Y. Wang), zheng.yanzhen@xjtu.edu.cn (Y.-Z. Zheng).
[1] These authors contributed equally to this work.

https://doi.org/10.1016/j.cclet.2025.110975
1001-8417/© 2026 Published by Elsevier B.V. on behalf of Chinese Chemical Society and Institute of Materia Medica, Chinese Academy of Medical Sciences.



Scheme 1. Synthetic routes for **1** and **2**.

bulky group-substituted imidazoline-2-imino ligands (Im^RN^-) obtained through complex multi-step organic synthesis, and these complexes exhibit excellent SMM performance with high U_{eff} of 1237 K and hysteresis loop opening temperatures up to 14 K [41]. As for the Dy–O complexes, Zhang *et al.* first reported two compounds $[Dy(BPA\text{-}TPA)(CH_3O/PhO)](BPh_4)_2{\cdot}nCH_2Cl_2$ using a bulky heptadentate [2,6-bis[bis(2-pyridylmethyl)amino]methyl]-pyridine (BPA-TPA) ligand to enwrap the Dy(III) ion and choosing CH_3O^- and PhO^- as axial strong field donors, exhibiting U_{eff} of 686 K and 469 K respectively and hysteresis loop opening temperatures up to 8 K [42].

To further enhance the magnetic axiality of Dy–O complexes, we perceived the stronger electron donors on the axial position and the weaker ancillary ligands are necessary. The previous work shown that ether type ligands are perfectly weak field equatorial ligands while alkoxides are suitable for enhancing the axiality [36,43–45]. Hence, we used this strategy to construct two "*pseudo*-mono-coordinate" Dy(III) complexes, $[Dy(O^tBu)(15\text{-}C\text{-}5)(THF)_2][I_3]_2$ **1** and $[Dy(1\text{-}AdO)(15\text{-}C\text{-}5)(THF)_2][I_3]_2$ **2**. Complexes **1** and **2** display the desired *pseudo*-mono-coordinate model with very strong axial $Dy–O_{alkoxide}$ bonding interaction and weak $Dy–O_{ether}$ bonds. As such both complexes exhibit enhanced SMM performance ($U_{eff} = 1054(6)$ K, $T_B^{hys} = 14$ K, $T_B^{ZFC} = 8$ K for **1**; $U_{eff} = 1028(9)$ K, $T_B^{hys} = 10$ K, $T_B^{ZFC} = 7$ K for **2**). Moreover, applying a 1 kOe field, the quantum tunneling of magnetization (QTM) process was effectively suppressed, and the relaxation times of **1** and **2** at 2 K increased by four orders of magnitude to 1216(10) s and 2368(13) s, respectively. Such results verifies the efficacy of the "*pseudo*-mono-coordinate" strategy to strengthen the SMM performance of Dy(III) complexes.

Crystals of **1** and **2** were grown by reacting 1 equiv. of metallic dysprosium, 3.5 equiv. of iodine (I_2), and 1 equiv. of KO^tBu or KO(1-Ad) in the presence of 15-C-5 (1 equiv.) in tetrahydrofuran (THF), followed by slow diffusion in THF/hexane (1:3) solution at room temperature (Scheme 1). The composition and molecular structures of **1** and **2** were identified by elemental analysis, infrared spectrum, and single crystal X-ray diffraction characterization (Supporting information).

Though **1** and **2** share the similar $[Dy(OL)(15\text{-}C\text{-}5)(THF)_2]^{2+}$ cationic components and two triiodide $[I_3]^-$ counterions they crystallize in different space groups. For **1** the complex crystallizes in the orthorhombic $P2_12_12_1$, which is chiral. For **2** it crystallizes in a more common monoclinic space group $P2_1/n$ (for detail, see Table S2 in Supporting information). We attribute this difference to the rotating feature of the tert–butyl group which may give additional helical element into the molecular crystal of **1** [46,47]. In addition to this difference the Dy(III) ions are both coordinated by a total of eight oxygen atoms, one from the alkoxides and seven from ancillary ligands, namely the η^5-chelating 15-crown-5 and two monodentate tetrahydrofuran molecules (Figs. 1a and b). The $Dy–O_{alkoxide}$ bond lengths are very short, namely 2.016(4) Å for **1** and 2.028(3) Å for **2** (Tables S3 and S4 in Supporting information), which are among the shortest up to date compared to other known dysprosium(III) complexes [43–45,48,49]. The slightly longer $Dy–O_{alkoxide}$ bond of **2** is attributed to the slightly larger steric hindrance of $1\text{-}AdO^-$. In contrast, the coordination of ether type ligands shows much longer $Dy–O_{ether}$ bond lengths ranging from 2.427(4) Å to 2.523(4) Å and from 2.416(3) Å to 2.509(3) Å for **1** and **2**, respectively. As such, the central Dy(III) ions are experiencing virtually a mono-coordinate crystal field as the negative charges are mainly focused on the alkoxides. Hence, both **1** and **2** are can be magnetically perceived as pseudo-mono-coordinate. As such, their ground energy splitting must be very similar to the diatomic model complex $[DyO]^+$ [37]. The shortest intermolecular Dy···Dy distances are 9.954(1) Å and 10.178(1) Å for **1** and **2**, respectively (Figs. S1 and S2 in Supporting information).

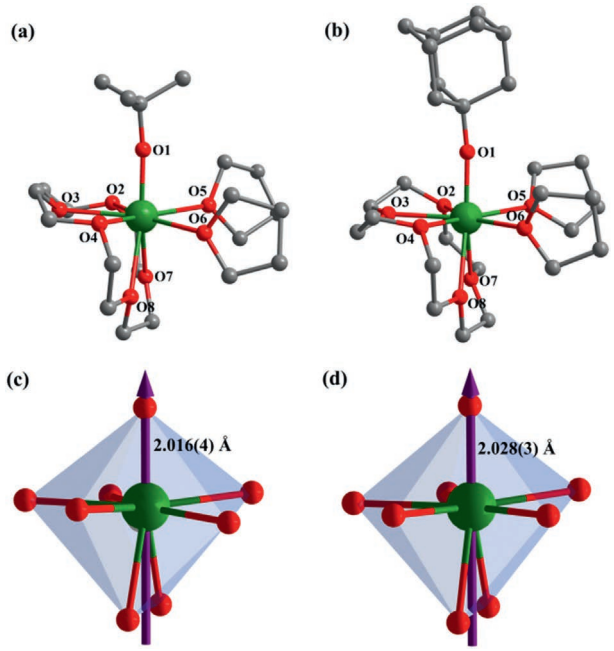


Fig. 1. Crystal structures for the $[Dy(OL)(15\text{-}C\text{-}5)(THF)_2]^{2+}$ cations in (a) **1** and (b) **2**. Side views of coordination polyhedra and calculated principal magnetic axes (depicted with purple arrow) for the ground doublet of Dy(III) ion in (c) **1** and (d) **2**. Colour codes: Dy, green; O, red and C, gray. All hydrogen atoms are omitted for clarity.

Variable-temperature direct current (dc) susceptibility data were conducted under a 2 kOe field from 300 K to 2 K. At 300 K, the $\chi_m T$ values are 14.06 and 14.14 cm^3 K/mol for **1** and **2**, respectively (Figs. S3 and S4 in Supporting information), aligning well with the theoretical values of 14.17 cm^3 K/mol for the free Dy(III) ion ($4f^9$, $^6H_{15/2}$, $S = 5/2$, $L = 5$, $g = 4/3$). Upon cooling, the $\chi_m T$ values for both decreases slowly down to 12 K, followed by a sharp drop to 6.09 and 7.01 cm^3 K/mol at 2 K, suggesting the presence of magnetic blocking at low temperature. Zero-field-cooled (ZFC) and field-cooled (FC) magnetic susceptibility were measured under 2 kOe field at 3 K/min. The ZFC–FC plots distinctly exhibit ZFC peaks at 8 K and 7 K for **1** and **2**, respectively (Figs. 2a and b). With a sweep rate of 200 Oe/s, magnetic hysteresis behavior were then investigated, and the butterfly-shaped hysteresis loops remain open up to 14 K and 10 K for **1** and **2**, respectively, indicating non-negligible QTM in the low-temperature region at zero field (Figs.

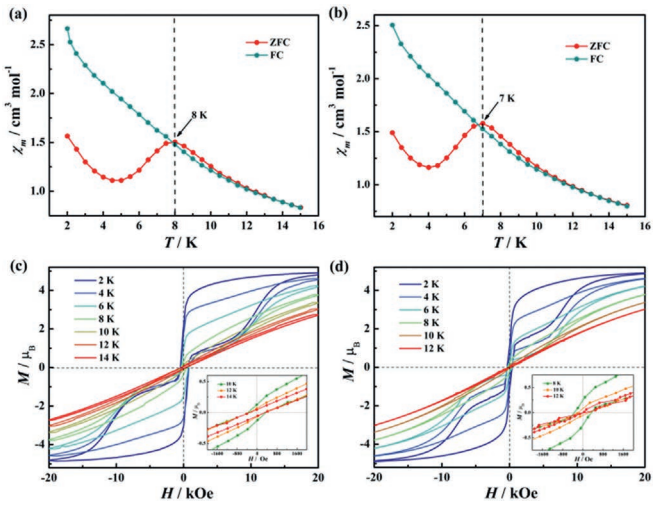


Fig. 2. Field-cooled (FC, dark cyan) and zero-field-cooled (ZFC, red) variable-temperature magnetic susceptibility for (a) **1** and (b) **2** under an applied field of 2 kOe from 2 K to 15 K (3 K/min). Magnetic hysteresis loops for (c) **1** and (d) **2** with an average sweep rate of 200 Oe/s. Insert: Magnification of hysteresis loops at selected temperatures.

2c and d). The somewhat higher blocking temperature of **1** than **2** is mainly attributed to the shorter Dy–$O_{alkoxide}$ bond. Meanwhile, the field (H) dependent magnetization (M) data were measured at 2−10 K from 0 to 50 kOe and the results reveal that the maximum M values are 5.10 and 5.13 μ_B at 50 kOe for **1** and **2**, respectively (Figs. S5 and S6 in Supporting information). In addition, the significant separations between the isofield curves in the reduced magnetization plots further demonstrate the presence of magnetic anisotropy.

Variable-frequency alternating current (ac) susceptibilities of **1** and **2** were measured in the zero field to probe the dynamic magnetic relaxation behavior (Figs. S7 and S8 in Supporting information). The pronounced frequency-dependent peaks of the out-of-phase (χ") ac susceptibility revealed characteristic signatures of SMMs, with well-defined maximum peak temperature (1000 Hz) of 58 K for **1** and 56 K for **2**. Temperature-dependent relaxation times were extracted by fitting the Cole−Cole plots of χ" *vs.* χ' with the generalized Debye model (Figs. S9 and S10, Tables S5 and S6 in Supporting information). The log-log plots of τ^{-1} *versus* T for **1** and **2** show three diverse correlations under zero external field (Fig. 3), corresponding to the temperature-dependent Orbach and Raman process as well as the temperature-independent QTM process. Consequently, these data can be fitted using the following equation.

$$\tau^{-1} = \tau_0^{-1} e^{-U_{eff}/T} + CT^n + \tau_{QTM}^{-1} \quad (1)$$

The best fitting parameters are $U_{eff} = 1054(6)$ K, $\tau_0 = 1.31(2) \times 10^{-12}$ s, $C = 4.87(4) \times 10^{-4}$ s^{-1} K^{-n}, $n = 3.5(2)$ and $\tau_{QTM} = 0.078(1)$ s for **1**; $U_{eff} = 1028(9)$ K, $\tau_0 = 1.43(3) \times 10^{-12}$ s, $C = 6.92(3) \times 10^{-5}$ K^{-n}, $n = 4.1(1)$ and $\tau_{QTM} = 0.065(2)$ s for **2** (Table 1).

Obviously, complexes **1** and **2** exhibit pronounced magnetic anisotropy, as evidenced by their U_{eff} values surpassing 1000 K. The comparatively higher U_{eff} value for **1** stems from the shorter axial Dy–$O_{alkoxide}$ bond. Nevertheless, the τ_{QTM} values <0.1 s indicate that high U_{eff} values do not afford them long relaxation times at low temperatures as expected, due to the significant impact of severe QTM.

Table 1
Fitting parameters for **1** and **2** at zero and 1 kOe field.

Complex	U_{eff} (K)	τ_0 (s)	C (s^{-1} K^{-n})	n	τ_{QTM} (s)
1 (0 Oe)	1054(6)	$1.31(2) \times 10^{-12}$	$4.87(4) \times 10^{-4}$	3.5(2)	0.078(1)
1 (1 kOe)	1054(7)	$1.50(3) \times 10^{-12}$	$3.31(2) \times 10^{-6}$	4.8(2)	/
2 (0 Oe)	1028(9)	$1.43(3) \times 10^{-12}$	$6.92(3) \times 10^{-5}$	4.1(1)	0.065(2)
2 (1 kOe)	1028(11)	$1.03(4) \times 10^{-12}$	$1.72(2) \times 10^{-6}$	5.1(1)	/

Moreover, we implemented field-dependent ac susceptibility measurements from 0 to 3 kOe at 30 K and obtained 1 kOe as the optimal external field for mitigating QTM (Fig. S11 in Supporting information). Under this applied field, we used ac susceptibility at higher temperatures to compile relaxation times (Figs. S12 and S13, Tables S7 and S8 in Supporting information). As the temperature decreases, the relaxation times progressively elongated, surpassing the detection threshold of the ac susceptibility measurements. Consequently, we used low-temperature dc magnetization decay measurements, from which relaxation times can be extracted by fitting the data to a stretched exponential function (Figs. S14 and S15, Tables S9 and S10 in Supporting information). We found that high-temperature relaxation times remained constant and low-temperature relaxation times were significantly prolonged (Fig. 3). At 2 K, the relaxation times of **1** and **2** are 1216(10) and 2368(13) s, respectively. These are about four orders of magnitude longer than those at zero field. Only considering the Orbach and Raman processes in Eq. 1, the best fits are also shown in Table 1. It is obvious that the presence of the optimal field does not affect the Orbach process while effectively suppressing the fast relaxation process.

To gain insight into the relaxation mechanism of **1** and **2**, complete-active-space self-consistent-field spin-orbit (CASSCF-SO) calculations were performed by Orca 5.0 program [50]. The geometries utilized in the calculations were directly extracted from their single crystal data without optimization. As expected, such crystal field environment affords the large energy splittings of 1213 and 1203 K for **1** and **2** which are originated from the ground term $^6H_{15/2}$ (Tables S11 and S12 in Supporting information). The ground Kramers doublet (KD) of them exhibits very strong magnetic axiality that its g tensors approach the Ising limit with $g_x = g_y = 0$, $g_z = 19.97$ and corresponding wavefunction is composed of pure $|\pm 15/2>$ state. As shown in Figs. 1c and d, the calculated principal magnetic axes for the ground KD of Dy(III) ion are both along the direction of axial Dy–$O_{alkoxide}$ in **1** and **2**, also verifying their uniaxial magnetic anisotropy. Then the electrostatic potential (ESP) from all coordinated O atoms was calculated based on Mulliken atomic charge (MAC) and corresponding Dy–O bond length (Table S13 in Supporting information). In terms of all similar MACs, it is evident that the ESP of oxygen atom on the alkoxide is largest which can be attributed to the shortest Dy–O distance. This result proves that the strong magnetic axiality in both complexes origins from the axial Dy–$O_{alkoxide}$ coordination mode.

For the first excited KD in **1** and **2**, it is located at 611 and 602 K higher than the corresponding ground KD, and can be well described as $m_J = |\pm 13/2>$. From the second excited KD on, the wavefunctions exhibit the admixture characteristic, together with the relatively large deviation angle of magnetic anisotropy axes relative to the ground KD (Tables S11 and S12). Additionally, the possible magnetic relaxation pathways were depicted in Figs. 4a and c, the transition magnetic moments of $\sim 10^{-4}$ μ_B between the ground KD is small enough which guarantees the zero-field SMM behaviour for **1** and **2**. Then reliable theoretical U_{eff} for both complexes were predicted by considering the thermal populations of tunneling rates for each KD based on Eqs. 2-4 [51,52]. k_i represents the demagnetization rate for each KD, and E_i refers to their relative energy height, while $k_{QT,i}$ is the tunneling rates within each KD where g_x, g_y and g_z are corresponding Landé factors. As shown in Figs. 4b and d, the calculated U_{eff} and relaxation contributions from various KDs are temperature dependent in the whole temperature regime which can be evidently segmented into three regions.

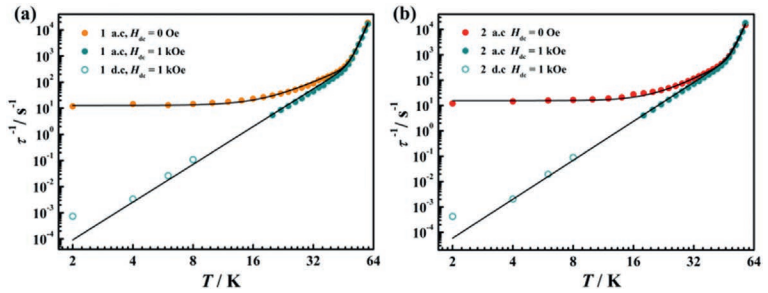


Fig. 3. Plots of natural log of τ^{-1} *vs.* *T* for (a) **1** and (b) **2** in zero and 1 kOe field. The solid lines are the best fits.

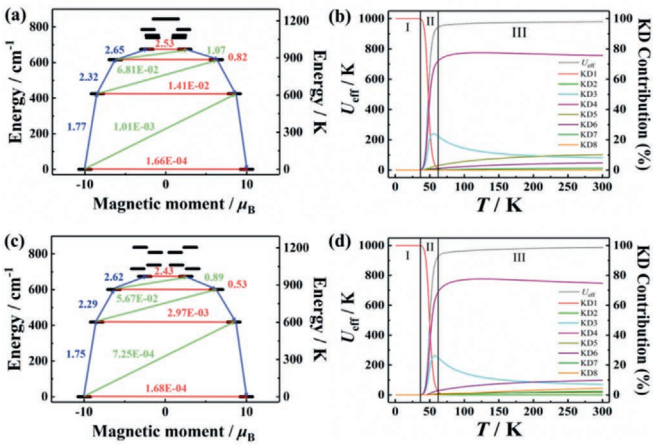


Fig. 4. Left: *Ab initio* calculated possible magnetic relaxation path diagrams for (a) **1** and (c) **2**. The horizontal red arrows represent the QTM/TA-QTM processes, while the non-horizontal ones show the spin-phonon transition paths. The numbers next to the arrows are averaged transition magnetic moments $((|\mu_X|+|\mu_Y|+|\mu_Z|)/3)$ in μ_B between the connecting pairs. Right: Predicted U_{eff} (black dotted lines) and relaxation contributions from various KDs (coloured solid lines) for (b) **1** and (d) **2**.

For region I, QTM within the ground KD dominates in the whole magnetic relaxation, affording the U_{eff} very close to zero. With the increment of temperature, the contributions of the ground KD decreases rapidly in region II while the ones for other excited KDs rise and get prominent, especially KD3 and KD4, which leads to the U_{eff} growing remarkably. In region III, Orbach relaxation is fully activated and the U_{eff} also becomes constant, together with the most relaxation contribution from KD4. Ultimately, the predicted saturation U_{eff} values for **1** and **2** are 980 and 987 K, which are agreement with the corresponding experimental ones.

$$U_{eff} = \sum_{i=1}^{n} \frac{K_{QT,i}(T)}{\sum_i k_i(T)} E_i \tag{2}$$

$$k_i(T) \propto \frac{exp\left(-E_i/k_BT\right)}{\sum_i exp\left(-E_i/k_BT\right)} k_{QT,i} \tag{3}$$

$$k_{QT,i} = \frac{g_x^2 + g_y^2}{2\left(g_x^2 + g_y^2 + g_z^2\right)^{1/2}} \tag{4}$$

In summary, we used ether type neutral ligands, 15-crown-5 and tetrahydrofurans, in conjunction with very basic alkoxide ligands O^tBu^- and 1-AdO^- to synthesize two *pseudo*-mono-coordinate Dy(III) complexes, which show SMM behaviour with high U_{eff} value exceeding 1000 K and opened magnetic hysteresis loops up to 14 K. Therefore, this work provides a new pseudo-mono-coordinate strategy to construct Dy(III)-alkoxide complexes with high SMM performance.

Declaration of competing interest

The authors declare that they have no known competing financial interests or personal relationships that could have appeared to influence the work reported in this paper.

CRediT authorship contribution statement

Wen-Jie Xu: Writing – original draft, Methodology, Formal analysis, Data curation. **Qian-Cheng Luo:** Software, Formal analysis, Data curation. **Yang Fang:** Data curation. **Chen-Jie Yuan:** Data curation. **Jin-Tao Lu:** Validation, Data curation. **Yuan-Qi Zhai:** Writing – review & editing, Supervision, Data curation. **Yu Wang:** Validation, Data curation. **Yan-Zhen Zheng:** Writing – review & editing, Supervision, Project administration, Funding acquisition.

Acknowledgments

This work was supported by the National Natural Science Foundation of China (Nos. 22375157, 52471016), the Medical-Engineering Cross Project of the First Affiliated Hospital of XJTU (No. QYJC02), Key Scientific and Technological Innovation Team of Shaanxi Province (No. 2020TD-001), State Key Laboratory of Electrical Insulation and Power Equipment (No. EIPE23405), Key Laboratory Construction Program of Xi'an Municipal Bureau of Science and Technology, and the Fundamental Research Funds for Central Universities (Nos. xtr052023002 and xzy012024057), "Scientists engineers" Team Building Project of Qin Chuang Yuan in Shaanxi Province of China (No. 2022KXJ-088) and the Programme of Introducing Talents of Discipline to Universities (No. B23025). We also thank the Instrument Analysis Center of Xi'an Jiaotong University.

Supplementary materials

Supplementary material associated with this article can be found, in the online version, at doi:10.1016/j.cclet.2025.110975.

References

[1] R. Sessoli, D. Gatteschi, A. Caneschi, M.A. Novak, Nature 365 (1993) 141–143.
[2] F.D. Natterer, W.Paul K.Yang, et al., Nature 543 (2017) 226–228.
[3] R. Sessoli, Nature 543 (2017) 189–190.
[4] L. Bogani, W. Wernsdorfer, Nat. Mater. 7 (2008) 179–186.
[5] S. Sanvito, Chem. Soc. Rev. 40 (2011) 3336–3355.
[6] M.N. Leuenberger, D. Loss, Nature 410 (2001) 789–793.
[7] A. Gaita-Ariño, F. Luis, S. Hill, E. Coronado, Nat. Chem. 11 (2019) 301–309.
[8] S. Thiele, F. Balestro, R. Ballou, et al., Science 344 (2014) 1135–1138.
[9] J.L. Liu, Y.C. Chen, M.L. Tong, Chem. Soc. Rev. 47 (2018) 2431.
[10] N.F. Chilton, Annu. Rev. Mater. Res. 52 (2022) 79–101.
[11] V.S. Parmar, D.P. Mills, R.E.P. Winpenny, Chem. Eur. J. 27 (2021) 7625–7645.
[12] C.A.P. Goodwin, F. Ortu, D. Reta, N.F. Chilton, D.P. Mills, Nature 548 (2017) 439–442.
[13] F.S. Guo, B.M. Day, Y.C. Chen, et al., Angew. Chem. Int. Ed. 56 (2017) 11445–11449.

[14] K.R. McClain, C.A. Gould, K. Chakarawet, et al., Chem. Sci. 9 (2018) 8492–8503.
[15] P.E. Evans, D. Reta, G.F.S. Whitehead, N.F. Chilton, D.P. Mills, J. Am. Chem. Soc. 141 (2019) 19935–19940.
[16] C.A. Gould, K.R. McClain, D. Reta, et al., Science 375 (2022) 198–202.
[17] J.C. Vanjak, B.O. Wilkins, V. Vieru, et al., J. Am. Chem. Soc. 144 (2022) 17743–17747.
[18] A.H. Vincent, Y.L. Whyatt, N.F. Chilton, J.R. Long, J. Am. Chem. Soc. 145 (2023) 1572–1579.
[19] G.K. Gransbury, S.C. Corner, J.G.C. Kragskow, et al., J. Am. Chem. Soc. 145 (2023) 22814–22825.
[20] Y.D. Wang, Q.C. Luo, Y.Z. Zheng, Angew. Chem. Int. Ed. 63 (2024) e202407016.
[21] F.S. Guo, B.M. Day, Y.C. Chen, M.L. Tong, Science 362 (2018) 1400–1403.
[22] J. Liu, Y.C. Chen, J.L. Liu, et al., J. Am. Chem. Soc. 138 (2016) 5441–5450.
[23] Y.S. Ding, N.F. Chilton, R.E. Winpenny, Y.Z. Zheng, Angew. Chem. Int. Ed. 55 (2016) 16071–16074.
[24] K.X. Yu, J.G.C. Kragskow, Y.S. Ding, et al., Chem 6 (2020) 1777–1793.
[25] X.L. Ding, Q.C. Luo, Y.Q. Zhai, et al., Chin. J. Chem. 40 (2022) 563–570.
[26] Y. Ma, Y.Q. Zhai, Q.C. Luo, Y.S. Ding, Y.Z. Zheng, Angew. Chem. Int. Ed. 61 (2022) e202206022.
[27] Q.C. Luo, Y.Z. Zheng, Trends Chem. 5 (2023) 869–872.
[28] X.L. Ding, Y.Q. Zhai, T. Han, et al., Chem. Eur. J. 27 (2021) 2623–2627.
[29] Z.H. Li, Y.Q. Zhai, W.P. Chen, Y.S. Ding, Y.Z. Zheng, Chem. Eur. J. 25 (2019) 16219–16224.
[30] Z.H. Zhu, C. Zhao, T.T. Feng, et al., J. Am. Chem. Soc. 143 (2021) 10077–10082.
[31] A.B. Canaj, S. Dey, C. Wilson, et al., Chem. Commun. 56 (2020) 12037–12040.
[32] Z.H. Zhu, C. Zhao, Q. Zhou, et al., CCS Chem. 4 (2022) 3762–3771.
[33] S.T. Liu, Y. Gil, C. Zhao, et al., Inorg. Chem. Front. 9 (2022) 4982–4989.
[34] S.K. Gupta, S. Dey, T. Rajeshkumar, G. Rajaraman, R. Murugavel, Chem. Eur. J. 28 (2022) e202103585.
[35] X. Zhong, D.Y. Li, C. Cao, et al., Inorg. Chem. 63 (2024) 21909–21918.
[36] W.J. Xu, Q.C. Luo, Z.H. Li, Y.Q. Zhai, Y.Z. Zheng, Adv. Sci. 11 (2024) 2308548.
[37] L. Ungur, L.F. Chibotaru, Phys. Chem. Chem. Phys. 13 (2011) 20086–20090.
[38] L. Norel, L.E. Darago, B.L. Guennic, et al., Angew. Chem. Int. Ed. 57 (2018) 1933–1938.
[39] A.B. Canaj, M.K. Singh, E.R. Marti, et al., Chem. Commun. 55 (2019) 5950–5953.
[40] B.K. Ling, Y.Q. Zhai, J. Han, T. Han, Y.Z. Zheng, Dalton Trans. 49 (2020) 6969–6973.
[41] R. Sun, C.Y. Li, Z.N. Huang, et al., CCS Chem. 7 (2025) 2054–2064.
[42] B. Zhang, Z.J. Cheng, Y.Y. Wu, et al., Chem. Sci. 13 (2022) 13231–13240.
[43] Y.S. Ding, W.J.A. Blackmore, Y.Q. Zhai, et al., Inorg. Chem. 61 (2022) 227–235.
[44] Y.S. Ding, T. Han, Y.Q. Zhai, et al., Chem. Eur. J. 26 (2020) 5893–5902.
[45] Y.S. Ding, K.X. Yu, D. Reta, et al., Nat. Commun. 9 (2018) 3134.
[46] M. Nespolo, A.H. Benahsene, J. Appl. Cryst. 54 (2021) 1594–1599.
[47] A. Matsumoto, S. Takeda, S. Harada, K. Soai, Tetrahedron 27 (2016) 943–946.
[48] Q.C. Luo, X.L. Ding, W.J. Xu, Y.Q. Zhai, Y.Z. Zheng, Chin. Chem. Lett. 36 (2025) 110304.
[49] W. Yang, G. Velkos, F.P. Liu, et al., Adv. Sci. 6 (2019) 1901352.
[50] F. Neese, Comput. Mol. Sci. 12 (2022) e1606.
[51] D. Aravena, J. Phys. Chem. Lett. 9 (2018) 5327–5333.
[52] B. Yin, C.C. Li, Phys. Chem. Chem. Phys. 22 (2020) 9923–9933.